energies

MDPI

Article

Analysis of the Icing Accretion Performance of Conductors and Its Normalized Characterization Method of Icing Degree for Various Ice Types in Natural Environments

Caijin Fan * and Xingliang Jiang

State Key Laboratory of Power Transmission Equipment & System Security and New Technology, Chongqing University, Shapingba District, Chongqing 400044, China; xljiang@cqu.edu.cn

* Correspondence: fancaijin@cqu.edu.cn; Tel.: +86-159-22887382

Received: 17 September 2018; Accepted: 7 October 2018; Published: 9 October 2018

Abstract: Icing degree in the severe icing regions for years is an important factor considered in the anti-icing design of transmission lines. However, there is currently no normalized characterization method for the icing degree of transmission lines, which can be used to record the severity of icing at icing areas over the years and guide the design of transmission lines. This study analyzes collision efficiency of water droplets with various diameters of conductors and investigates the ice accretion law of transmission lines with various diameters under four natural ice types. Therefore, the normalized method of standard ice thickness instead of various ice morphologies is creatively used to characterize icing degree of transmission lines and a lot of field tests which have been done at six natural ice observation stations have verified the effective of the method. The results have shown that: The diameters of conductor and the droplet significantly affect collision efficiency; the relation of standard ice thickness with diameter of conductors for four typical ice types complied with the law of power function. The results can provide important references for the design and external insulation selection of transmission lines in ice region.

Keywords: normalized characterization method; natural icing tests; ice types; collision efficiency; transmission lines

1. Introduction

Atmospheric icing of structures, such as transmission lines [1], marine vessels and offshore structures [2,3], aircraft icing [4], and so on, is a complex physical phenomenon that is affected by factors including meteorological condition, terrain, elevation, etc. [1]. Extra/Ultra-high voltage (EHV/UHV) transmission lines inevitably pass through high altitude and a typical micro-meteorological icing area, which may result in huge economic loss due to a series of electrical and mechanical faults of icing flashover [5–8], conductor galloping [9–11], asynchronism of ice shedding [12–14], and even broken line [15–17]. At present, the methods of anti-icing and de-icing, such as super-hydrophobic coatings, short circuit method to melt ice [18], and mechanical de-icing, are costly, inefficient, and difficult to maintain. Various ice theories of transmission lines are proposed but lack of scientific design theory and effective anti-icing method of transmission lines [19] maybe restrict the development and popularization of EHV/UHV transmission.

The research of icing lines has always been a hot problem of the scientific field and has received extensive attention from researchers. In recent decades, several ice growth models have been established focus on the ice mass by extensive theoretical and testing researches at home and abroad. The typical ice growth model which is widely recognized for structures considers that ice covering

includes three processes which are collision, combination, and freezing, and the growth rate of the ice amount is proportional to the velocity of water droplet and the effective cross-sectional area of the structure.

Due to the randomness of natural environmental factors and torsional properties of transmission lines, ice morphologies of which conductors can be measured by online technologies [20,21] may be crescent-shaped, elliptical-shaped, or other complex ice shapes [1,20] and on-line monitoring of the icing degree of transmission lines (including ice morphologies and ice thickness) [22–24] plays an important role in safe operation in power grid. Based on the mathematical model of ice growth in two-dimensional lines or wings, one of their ice morphologies can be simulated by calculating the droplet flow trajectory around the circular conductor. Therefore, simple ice morphology of conductors was tested, which showed that the ice thickness with windward surface of the conductors was inversely proportional to the diameter in early stage of icing [25]. The diameter correction coefficient of the elliptical-shaped iced conductors has been modified based on the equivalent diameter of elliptical ice [26,27], currently; furthermore, for complex ice morphologies, the relationship between diameter correction coefficient and diameter of conductors was studied for conductors with different diameters based on rime, mixed ice, and glaze tests in artificial climate chamber [28].

Although the research about the iced conductors has been investigated over the past several decades, it is limited by the scarcity of natural ice test platform of full-scale transmission lines, mainly because the construction of the ice platform is difficult and costly. Therefore, most of the ice tests of conductors are carried out in artificial climate chambers at present. Research in Reference [29] studied the ice growth characteristics of on conductors with diameters ranging from 0.25 to 1.75 inches by measuring the ice thickness on the top and side of each conductor and the length of icicle based on artificial icing tests. The results show that when the diameter is in the range of 1–1.75 inches, the equivalent ice thickness of test conductors is the same; the ice thickness of conductor with diameter being 0.25 inch is 20% thicker than that of a conductor with a diameter of 1 to 1.75 inches, while their icing morphologies are almost the same considered to be formed under static environmental conditions, because the process of the ice conductors which are only 46 inches long without the torsional properties of long span transmission lines involves glaze only instead of hard rime, mixed ice, and soft rime because of randomness of environment. Accordingly, the research in [29] is not suitable for other weird ice morphologies of transmission lines with different ice types in natural environment, but so far there has been no unified approach for effectively characterizing icing degree.

The purpose of this paper is to possess a general characterizing method for icing degree of transmission lines, which can provide an accurate and effective field measurement method, and under four typical ice types, emphasis is placed on the influence of the diameters of conductors on standard ice thickness using normalized characterization method based on the field test results of six natural ice observation stations, such as Xuefeng mountain, Liupanshui. The law of the iced conductor is to some extent applied in the design of transmission lines at icing areas.

2. Test Platform and Methods

2.1. Test Platform

In terms of the general policy of Chinese power system development, which is "power transmission from west to east, mutual supply between south and north, nationwide interconnection", natural icing tests were conducted at six natural ice test observation stations near the Yangtze River Basin, namely Liupanshui, Huangmaogen, Jianshi, Badong, Xuefeng, and Qijiang, which are located in the transmission lines corridor along the "power transmission from west to east". There are north-south mountain ranges in the territory, which have an average altitude of 500–1900 m. It is the only way for transmission lines in the "power transmission from west to east" project in China, where are numerous rivers flowing into the Yangtze River from north to south. Therefore, field measurement stations are located in the area where landforms fluctuate and rivers

intersect, forming a wide range of micro-meteorological and micro-topographic areas. There are four ice types, such as glaze, hard rime, mixed ice, and soft rime, which are common in transmission lines in different periods.

The cross-sectional shape of the iced conductor in natural ice test base is affected by wind speed, the supercooled water droplets size, and torsional stiffness of conductors, among which torsional stiffness of conductors plays a decisive role, and Xuefeng mountain natural icing test base is shown in Figure 1. Conductors in artificial ice tests are short and torsional stiffness of conductors is high. Therefore, the cross-sectional shape is generally elliptical or wing shaped. However, the actual transmission line which is prone to twisting for the iced conductors has a large span and small torsional stiffness, which can truly reflect the ice morphology of transmission lines under different ice types. Some typical icing morphologies observed in field sites are shown in Figure 2. The thickest part of the ice layer is generally on windward side, while the thinnest part of the ice layer is on leeward side.

Figure 1. Xuefeng mountain natural icing test base.

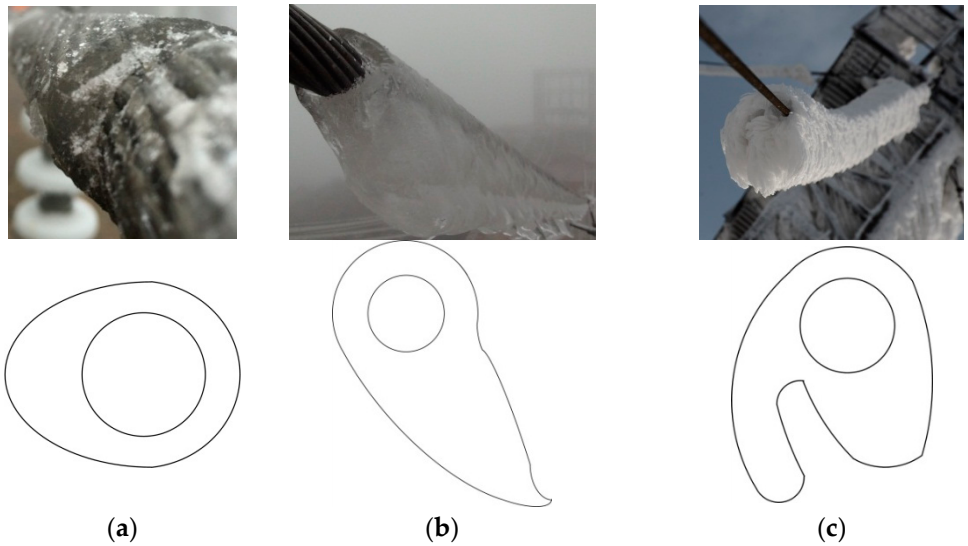

Figure 2. *Cont.*

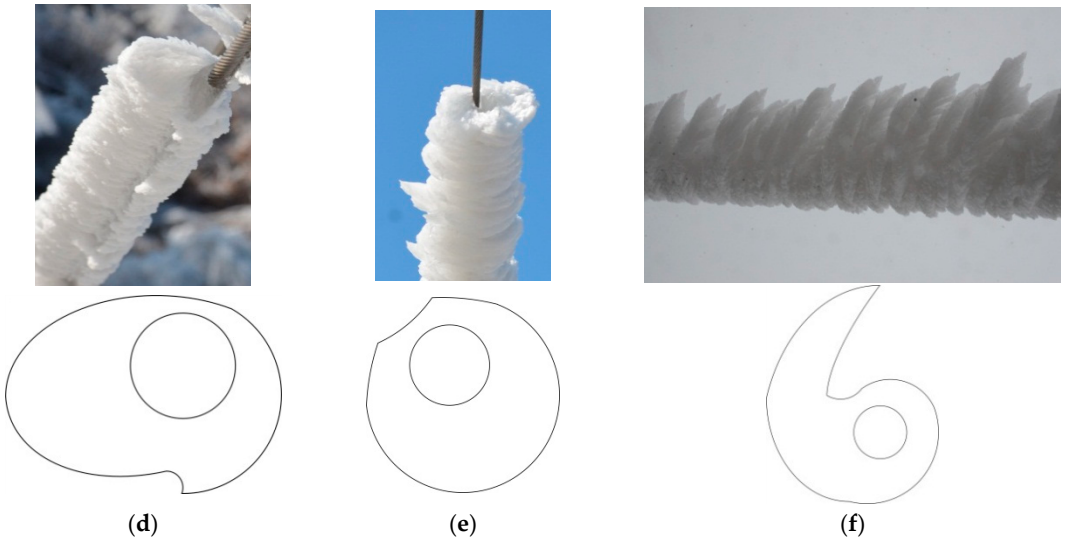

Figure 2. Typical ice profiles of the iced conductors (**a**) Crescent shape; (**b**) Wing shape; (**c**) Wing shape and eccentric circle; (**d**) Eccentric oval shape; (**e**) eccentric round shape; (**f**) Wing shape and round shape.

2.2. Test Methods

In order to study the ice growth performances of conductors with different diameters, which are 5, 10, 15, 20, and 25 mm, respectively, test samples are used for icing tests at the ice observation station, which are numbered 1, 2, 3, 4, and 5, respectively. The test sample conductors were suspended between two iron towers for icing tests, and the span between the two towers exceeds 80 m, as shown in Figure 1.

The methods for characterizing the icing degree of transmission lines are usually to measure the maximum and minimum ice thickness of conductors [30], or to measure the three ice parameters, such as the length of icicle and the ice thickness at the top and side of conductors [29]. However, they are approximately methods for characterizing the icing degree of transmission lines, because ice density is different with four typical ice types and there is also a big difference in ice morphology. Therefore, during the natural icing tests, the two-dimensional cross-sectional shape of the actual ice shape of conductors is recorded with a pen, as shown in Figure 3, and the two-dimensional cross-sectional area (S) of the actual ice morphology is calculated using AutoCAD software. Finally, the complex uneven ice morphologies with different densities and shapes are normalized and characterized as standard cylindrical ice with a density of 0.9 g/cm^3, which is called standard ice thickness. Therefore, the standard ice thickness of conductors was analysed involving the Equation (1) mathematical transposition, and the specific method is as follows.

The flow diagram of the field tests is shown in Figure 3, and the test process is mainly divided into three steps. Furthermore, more detailed operation processes can be divided: (1) To facilitate observation and recording of the cross-sectional shape of the iced conductor, cut a fracture in the ice layer around the conductor with a small saw; (2) Take a blank sheet of paper to drill a hole in the middle of the paper that has the same diameter as the conductor, cut a channel from the edge of the paper toward the round hole, place the conductor in a round hole in the middle of the white paper, and place the white paper flatly on the fracture of the iced conductor; (3) Put the white paper on it and trace the ice cross-sectional shape of conductor along the edge of the ice-covered cross section; (4) Import the ice-covered cross section into AutoCAD software to obtain the ice-covered cross-sectional area S;

(5) According to the Equation (1), calculate the standard ice thickness d of the cylindrical ice-covered conductor with a density of 0.9 g/cm^3.

$$d = \sqrt{R^2 + \frac{\gamma}{0.9}(\frac{S}{\pi} - R^2)} - R \quad (1)$$

where d is the standard ice thickness, mm; R is the radius of the wire, mm; γ is the actual ice density, g/cm^3; S is the measured cross-sectional area of the iced conductor, mm^2.

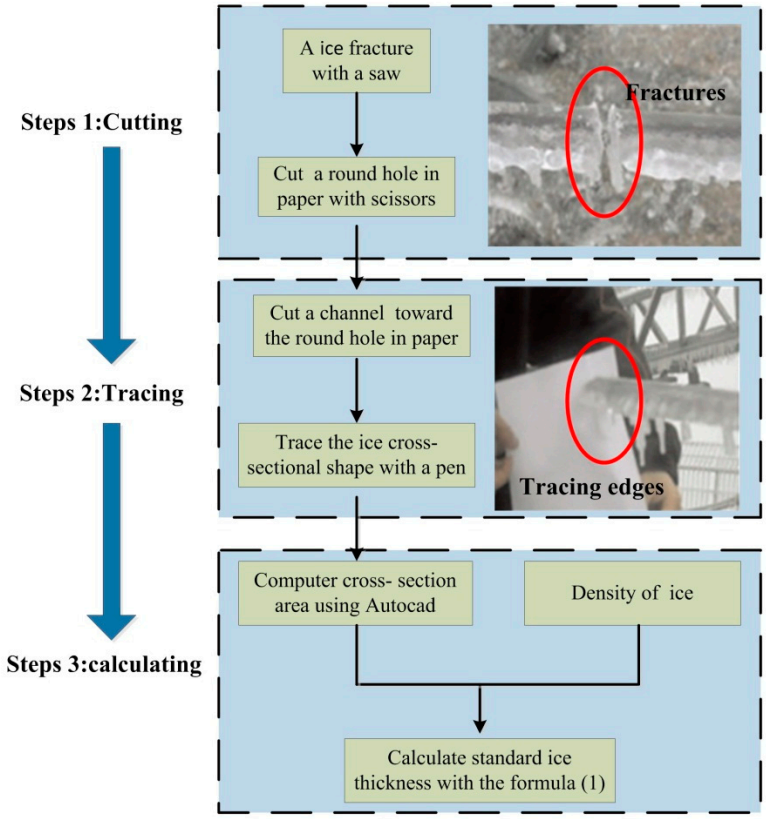

Figure 3. Flow diagram of standard ice thickness of the test conductors.

3. Influence Mechanism of Diameter and Droplet Size on Conductor Icing

Conductor icing is a physical phenomenon that conductor catches particles in the air and then release latent heat and freeze, and these particles can be either liquid, solid, or a mixture of ice and water. The relative orders of magnitudes of inertia and air resistance depend on droplet size, air flow rate, and the size of object itself. Collision efficiency is defined as the ratio of the amplitude water droplets colliding with objects and the diameter of the iced object. As shown in Figure 4, assume that the ordinate of the droplet in the airflow is y_0 at infinity (point Q) from the target object, when the droplet moves from Q to the P at the cylinder, and its velocity direction at point P is just along the tangent of the cylinder. Collision efficiency can be expressed as,

$$E = \frac{y_0}{R} \quad (2)$$

where y_0 is the ordinate of water droplets, mm; R is Radius of the conductor, mm.

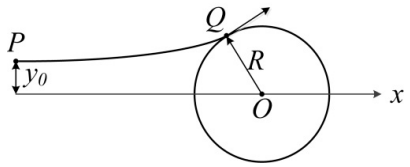

Figure 4. Moving trajectories of the droplet.

As shown in Figure 4, the droplets between the streamline QP and the x-axis will collide with the target object. Assuming rebound water droplets and direct freezing of the surface of the iced conductor, that is capture rate and freezing rate are equal to 1, collision efficiency (E) directly affects ice thickness and ice morphology. Therefore, the growth process of the surface of the conductor is related to collision efficiency of water droplets. E indicates the overall collision efficiency during the icing tests of the iced conductor and is dimensionless, which is parameterized through Stokes constant K and Langmuir constant φ. Finstad et al. [31] put forward the following mathematical equation about the collision coefficient α_1 based on conclusions in

$$\alpha_1 = A - 0.028 - C(B - 0.0454) \tag{3}$$

where

$$A = 1.066K^{-0.00616}\exp(-1.103K^{-0.688}) \tag{4}$$

$$B = 3.641K^{-0.498}\exp(-1.497K^{-0.694}) \tag{5}$$

$$C = 0.00637(\varphi - 100)^{0.381} \tag{6}$$

$$K = \frac{\rho_w {d_p}^2 v}{9\mu D} \tag{7}$$

$$\varphi = \frac{{R_e}^2}{K} \tag{8}$$

$$R_e = \frac{\rho_a v d_p}{\mu} \tag{9}$$

In the Equations (4)–(9), d_p is the diameter of the droplet, D is the diameter of the conductor, ρ_w is the density of the droplet, μ is the absolute viscosity of the air, and ρ_a is the air density.

Based on the Equations (3)–(9), the function of collision efficiency α_1 can be programmed by Matlab software. As shown in Figure 5, 192 computational cases (any combination of three sets of diameter of the conductor D (0.05–0.6 m), diameter of the droplet d_p (10–500 μm), and wind velocity v (0.1–10 m/s)) were calculated and their experimental data points of collision efficiency were shown. Therefore, through programming calculations by Matlab software, the influence of the diameter of the conductor and droplet size on collision efficiency was analyzed.

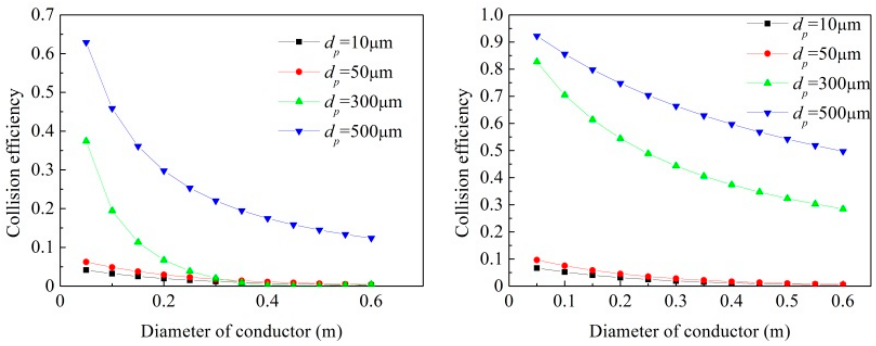

(**a**) v = 0.1 m/s (**b**) v = 1 m/s

Figure 5. *Cont.*

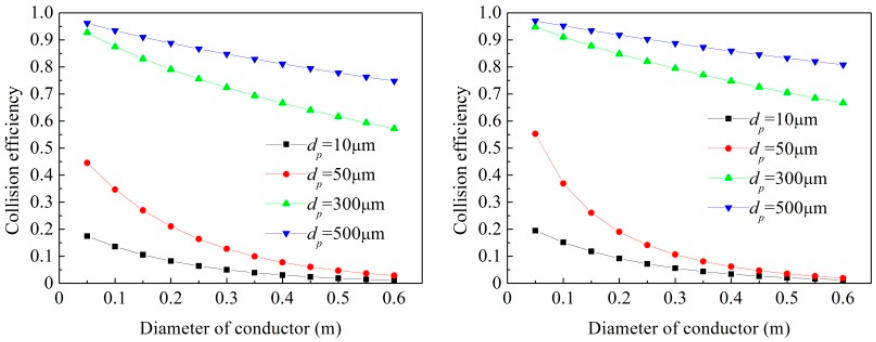

Figure 5. Collision efficiency of the water droplets with the different diameters of conductors.

The four graphs in Figure 5 show the change relation between collision efficiency and the diameter of the conductor with different wind speed and droplet sizes.

When droplet size is less than 50 μm in diameter, collision efficiency of large diameter conductor is almost zero (for example, D = 40 mm, d_p = 10 μm), because of small water droplets around the large diameter conductor experiencing violent roll flowing. When droplet size is larger than 300 μm in diameter, wind speed has a great impact on collision efficiency. Collision efficiency of water droplets is small in non-wind condition (less than 1 m/s), and collision efficiency increases with the increase of wind speed, because the double effect (wind speed and the inertia of water droplet) on water droplets, roll flowing around the conductor is weakened, which accelerates the collision between water droplets and conductors.

The following conclusions can be drawn from Figure 5:

(1) Collision efficiency has a nonlinear relationship with the diameter of the conductor. Collision efficiency decreases rapidly with the increase of the diameter of conductors, and it eventually becomes saturated.

(2) When droplet size is less than 50 μm in diameter, wind speed only impacts on collision efficiency of conductors with diameter of less than 0.1 m, while when droplet size is larger than 300 μm in diameter, the effect of wind speed on collision efficiency gradually increases.

(3) When wind speed and the diameter of the conductor remain unchanged, the larger the diameter of water droplet, the greater the corresponding collision efficiency is. For example, when wind speed is 5 m/s and the diameter of the conductor is 25 mm, the corresponding collision efficiency reaches maximum (0.867) with the diameter droplet being 500 μm, and that is a minimum (0.064) with the diameter droplet being 10 μm.

4. Test Results and Analysis

4.1. Field Test Results

Based on six natural ice test observation stations selected by Chongqing University along the Yangze River, the field stations are typical micro-meteorological and micro-topographic characteristics, which may cover four typical ice types at different periods. Researchers of Chongqing University had conducted the tests of the iced conductors based on actual environmental conditions at that time at test stations, when icing may last two or three days. The parameters such as the ice amount of the unit length line, ice density, and ice morphology are measured in the corresponding time. The standard ice thickness of conductors with different diameters under various typical ice types converted in accordance with the standard ice thickness method is shown in Table 1, where the height of the test conductors above ground is 2.0 m. *G*, *H*, *M*, and *S* are glaze, hard rime, mixed ice, and soft rime, respectively. Some typical ice shapes of conductors are shown in Figure 2.

Table 1. Standard ice thickness of conductors for typical ice types tested in Natural test stations.

Diameter (mm)	Standard Ice Thickness (mm)									
	Liupanshui				Huangmaogen				Jianshi	
	G	*H*	*M*	*S*	*G*	*H*	*M*	*S*	*G*	*S*
5	8.3	37.2	23.5	30.2	25.2	30.6	41.5	17.3	6.7	27
10	5.7	33.1	19.6	25.9	22.1	27.3	36.2	14.4	4.4	23.3
15	4.6	30.8	17.5	24.1	19.2	24.8	32.9	12.9	3.5	21.1
20	4	28.7	16.4	22.6	18.4	23.9	30.5	11.6	2.8	19.5
25	3.7	27.6	15.6	21.3	16.8	22.3	29.1	10.9	2.7	18.6
Diameter (mm)	**Badong**			**Xuefeng**					**Qijiang**	
	G	*H*	*S*	*G* in 2008	*G* in 2009	*H*	*M*	*S*	*G*	*S*
5	11	13.2	20.7	15.5	20.1	39.4	31.8	29.3	5.3	4.1
10	8	9.6	17.4	12.5	16.7	34.7	28.3	25.3	3.1	2.2
15	6.7	8.7	15.5	10.6	15.2	31.2	26.5	22.7	2.3	1.7
20	6	7.6	14.1	10.2	13.4	29.8	23.9	21.2	1.9	1.3
25	5.4	7	13.3	9.7	12.6	27.2	22.8	19.9	1.8	1.1

4.2. Effect of Ice Type on Ice Performances of Conductors

Due to global energy network being constructed by UHV transmission lines in China, much more transmission lines pass through ice-covered areas such as those with high altitude, micro-topography, and micro-meteorology. As shown in Figure 2, for the same diameter of the conductor, ice types in ice-covered regions have a significant influence on the ice morphologies of the conductor. Specifically, the ice morphology for glaze is mainly crescent-shaped in early stage of icing, while that for other ice types is more wing-shaped. Ice morphologies with various ice types are regular in early stage of icing. Because of the randomness of the environmental parameters such as droplet size, ambient temperature, and wind speed, the surface of the conductors are covered with non-uniform ice for irregular ice shapes eventually.

Based on the standard ice thickness of the reference conductor with a diameter of 5 mm, the reduction of the standard ice thickness of conductors relative to that of the reference conductor (hereinafter short for the relative reduction) is calculated as follows:

$$\triangle d = \left| \frac{d_i - d_1}{d_1} \right| \times 100\%, i = 1, 2, 3, 4, 5 \tag{10}$$

where d_i is the standard ice thickness of the ith conductor.

The relative reduction of different ice types can be calculated with Equation (4). The conductor icing characteristics of different diameters with four ice types in Liupanshui are shown in Figure 6. Because of randomness of the environmental parameters (such as real-time change of rainfall duration, droplet size, and wind speed) during the ice tests, and the icing tests with four ice types was tested at different periods. Therefore, the standard ice thickness with four ice types cannot compare with each other.

As shown in Figure 6, their changing law with diameter is similar. For a conductor with a diameter of 25 mm, the reduction of the ice thickness of glaze is the largest (55.42%) for the four kinds of ice types, while that of soft rime is the smallest (25.81%). The following conclusions can be reached:

(1) Ice types have a great effect on the ice morphologies of icing lines. Ice shape for glaze over the conductor shows a crescent or elliptical shape, while that of other ice types of icing lines is wing-shaped in early stages of icing.

(2) Under different ice types, the trend of the standard ice thickness with the diameter of the conductor is similar, and it decreases rapidly with increasing of the diameter of conductor and gradually becomes saturated.

(3) The relative reduction of different ice types increases with the increase of the diameter, and the relative reduction increases very little with a further increase of the diameter when the diameter exceeds a certain degree regardless of ice type.

(4) The typical ice thickness of 25 mm diameter conductor is smaller than that of 5 mm diameter conductor for the four ice types, and the corresponding relative reductions for glaze, hard rime, mixed ice, and soft rime are 55.42%, 33.62%, 29.47%, and 25.81%, respectively.

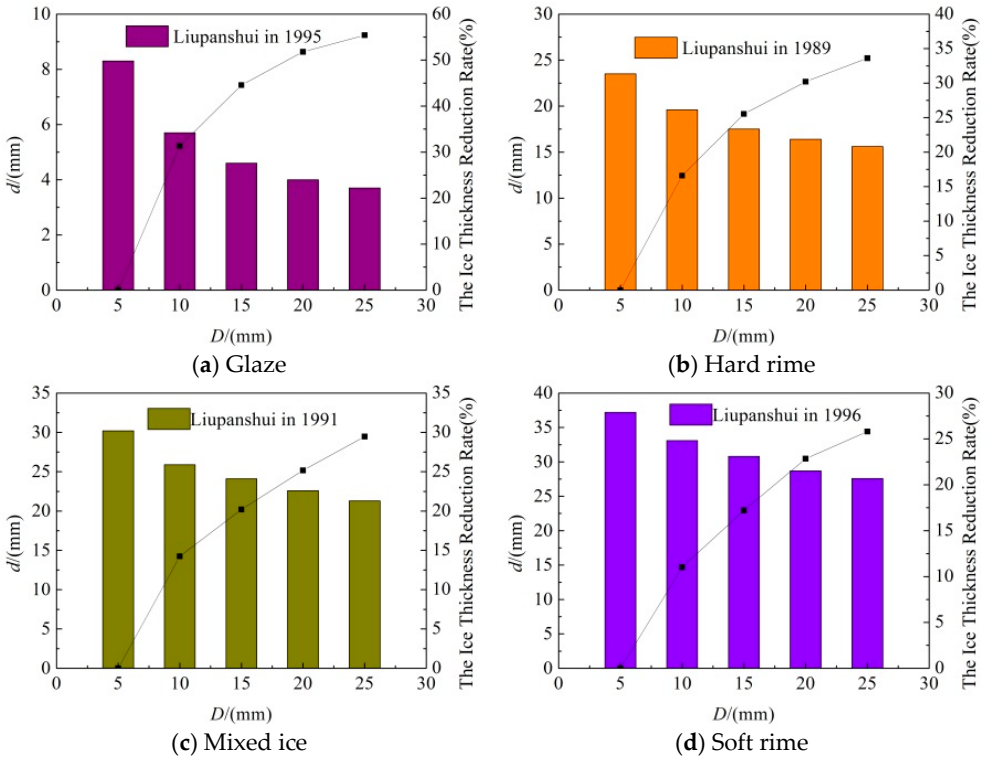

(**a**) Glaze (**b**) Hard rime

(**c**) Mixed ice (**d**) Soft rime

Figure 6. Standard ice thickness and its reduction with different diameters of conductors at Liupanshui station.

4.3. Effect of the Diameter of Conductors on the Performances of Natural Icing Lines

A unified representation of the icing degree of transmission lines with different ice types was discussed with the standard ice thickness method. The standard ice thickness of transmission lines with different diameters has important reference value for the design of overhead transmission lines in icing area. Therefore, it is necessary to further study the influence of the diameter of the conductors on the standard ice thickness of the conductors with typical ice types. According to the standard ice thickness method, the standard ice thickness of different diameters of conductors is calculated based on the test results of six natural ice observation stations, as shown in Figure 7. The standard ice thickness with the different diameters of conductors is very similar at each icing observation station, and under the same environmental conditions, the larger the diameter of conductor, the thinner the standard ice thickness is. Therefore, the relationship between standard ice thickness and the diameter of conductors is fitted using the power function formula, and the formula is as follows,

$$d = aD^{-b} \tag{11}$$

where d and D are standard ice thickness and the diameter of conductor, respectively; a, b are constants; a indicates the icing degree of conductors; b is characteristic index.

Through the regression analysis of the test results, the values of a and b are obtained, which are all greater than 0. As shown in Table 2, under the typical ice types, standard ice thickness and the diameter of the conductor have a power exponent of a negative index. As shown in Figure 7,

because the environmental parameters and test durations are randomly changed in each natural ice test, parameter value *a*, *b* of each group is different, as shown in Table 2. *G*, *H*, *M*, and *S* are glaze, hard rime, mixed ice, and soft rime, respectively.

As shown in Table 2, The conclusions are as follows:

(1) There was a typical power function relationship between standard ice thickness of the conductor and the diameter of the conductor for typical ice types, and the characteristic index b is less than 1, for example, the calculation results for glaze, hard rime, mixed ice, and soft rime in Liupanshui are $d = 19.07D^{-0.520}$, $d = 35.56D^{-0.258}$, $d = 42.45D^{-0.212}$, $d = 50.33D^{-0.185}$, respectively.

(2) At the same of the diameters of the iced conductors, standard ice thickness of the iced conductors for the four ice types may have a maximum value, which is mainly related to the icing environmental conditions and the icing test time.

Table 2. Fitting results of standard ice thickness with different diameters of conductors.

					$d = aD^{-b}$				
Liupanshui	***G***	***H***	***M***	***S***	**Huangmaogen**	***G***	***H***	M	***S***
a	19.07	35.56	42.45	50.33	a	59.51	41.83	37.74	27.49
b	0.520	0.258	0.212	0.185	b	0.221	0.191	0.245	0.285
R^2	0.9976	0.9986	0.9973	0.9945	R^2	0.9959	0.9886	0.9784	0.9959
Badong	***G***	***H***	***S***	**Xuefeng**	***G* in 2008**	***G* in 2009**	***H***	***M***	***S***
a	22.36	32.35	24.62	a	56.52	44.47	32.00	43.19	25.16
b	0.443	0.274	0.393	b	0.219	0.202	0.285	0.238	0.304
R^2	0.9992	0.9968	0.9894	R^2	0.9824	0.9704	0.9895	0.9961	0.9841
Jianshi	***G***	***S***			**Qijiang**	***G***	***S***		
a	17.40	39.41			a	16.91	15.44		
b	0.594	0.232			b	0.725	0.827		
R^2	0.9955	0.9972			R^2	0.9936	0.9968		

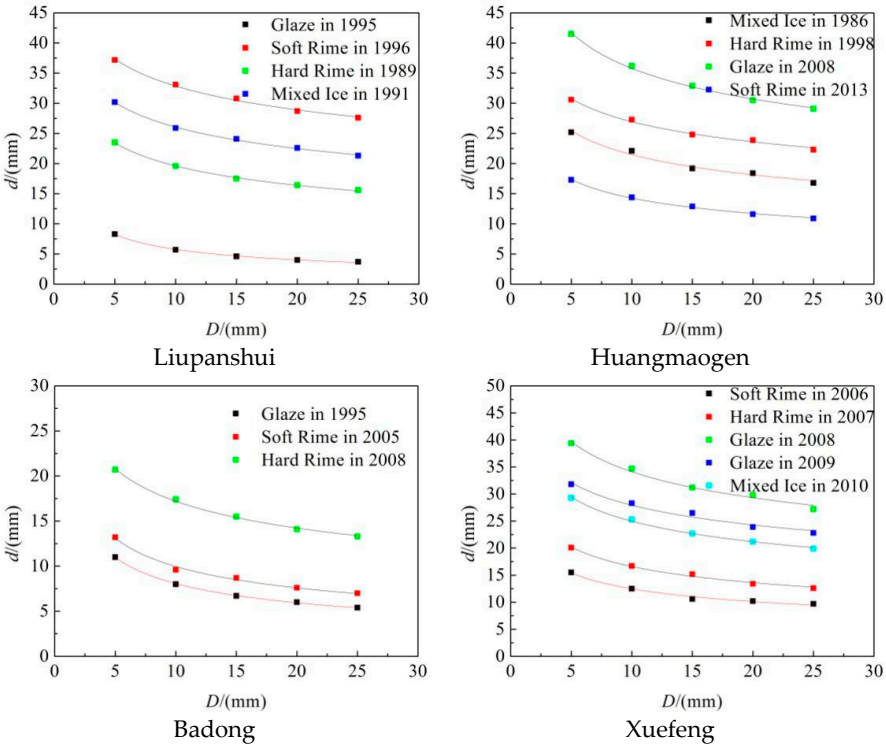

Figure 7. *Cont.*

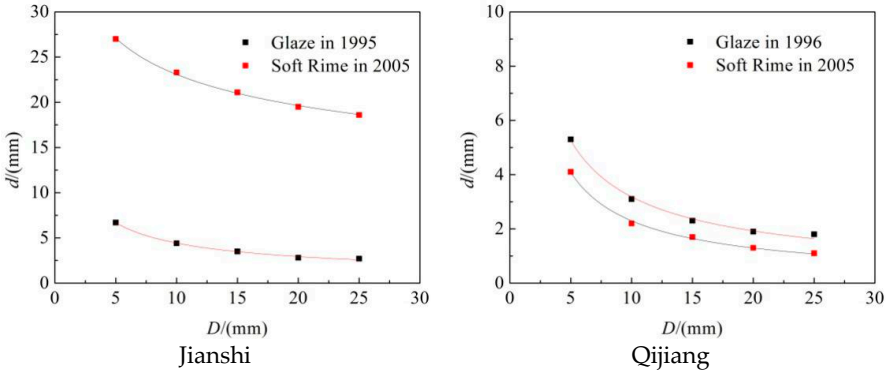

Figure 7. Fitting curves of each natural icing observation station using negative power function.

5. Conclusions

In the present study, ice mechanism of conductors with different diameters is investigated. The collision characteristics of water droplets with different diameter of particles are calculated by programming, and the performances of the iced conductor with different diameters for the four ice types are analyzed based on icing test results in natural ice observation stations. The conclusions are as follows:

(1) The ice morphologies of the iced conductors for natural ice types are very irregular and non-uniform. The complex ice shapes can be simplified as standard cylindrical ice with a density of 0.9 g/cm^3 using the standard ice thickness method, and a new idea for field measurement of transmission lines icing is presented in cold regions. It is easy to record the icing degree of transmission lines at various icing areas, which can provide an important reference for the design for overhead transmission lines at icing areas.

(2) For different droplet sizes, the changes on collision efficiency which with the diameter of the conductor decreases with increasing diameter of the conductor showed the same trend, and collision efficiency increases very little with a further increase of the diameter when the diameter exceeds a certain degree regardless of droplet sizes. When wind speed and the diameter of conductors are constants, collision efficiency increases with the increase of droplet size.

(3) The ice type has a great influence on the actual icing profile of the iced conductor. The ice morphologies in early stage of icing with various ice types are regular (crescent-shaped or wing-shaped), and the surface of the conductors will covered with non-uniform ice for irregular ice shapes eventually. The relative reduction for different ice types increases rapidly with increasing of the diameter of conductor and gradually becomes saturated.

(4) For the typical ice types, standard ice thickness and the diameter of the conductor have a power exponent of a negative index, and the characteristic index is less than 1, for example, the calculation results for mixed ice in Liupanshui is $d = 42.45D^{-0.212}$. Same as the diameter of conductors, the standard ice thickness for the four ice types may have a maximum value. Therefore, the natural icing law of conductors which has important engineering significance for anti-icing applied in large diameter conductors in icing area is further studied.

Author Contributions: X.J. conceived and designed the experiments; C.F. and X.J. performed the experiments; C.F. and X.J. analyzed the data; C.F. wrote the paper.

Funding: This work was supported financially by the National Natural Science Foundation of China (Grant No. 51637002), and graduate scientific research and innovation foundation of Chongqing, China (No.CYB16019).

Conflicts of Interest: The authors declare no conflict of interest. The founding sponsors had no role in the design of the study; in the collection, analyses, or interpretation of data; in the writing of the manuscript, and in the decision to publish the results.

Nomenclature

A. Variable	
d	Standard ice thickness (in millimeters).
D	Diameter of the conductor (in millimeters).
d_p	Diameter of the water droplet (in millimeters).
Δd	Reduction of standard ice thickness.
E	Collision efficiency.
R	Radius of the conductor (in millimeters).
S	Cross-sectional area of the iced conductor (in mm^2).
v	Wind velocity (in meters per second).
y_0	The ordinate of water droplets (in in millimeters).
α_1	Collision coefficient.
γ	Density of ice g/cm^3.
ρ_a	Air density g/cm^3.
ρ_w	Density of the droplet g/cm^3.
μ	Absolute viscosity of the air mm^2/s.
B. Abbreviation	
EHV	Extra-high voltage.
UHV	Ultra-high voltage.
G	Glaze.
H	Hard rime.
M	Mixed ice.
S	Soft rime.

References

1. Jiang, X.; Yi, H. *Ice Accretion on Transmission Lines and Protection*; Chinese Electric Power Press: Beijing, China, 2002. (In Chinese)
2. Dehghani-Sanij, A.R.; Dehghani, S.R.; Naterer, G.F.; Muzychk, Y.S. Sea spray icing phenomena on marine vessels and offshore structures: Review and formulation. *Ocean Eng.* **2017**, *132*, 25–39. [CrossRef]
3. Dehghani-Sanij, A.R.; Dehghani, S.R.; Naterer, G.F.; Muzychka, Y.S. Marine icing phenomena on vessels and offshore structures: Prediction and analysis. *Ocean Eng.* **2017**, *143*, 1–23. [CrossRef]
4. Gao, H.; Rose, J.L. Ice detection and classification on an aircraft wing with ultrasonic shear horizontal guided waves. *IEEE Trans. Ultrason. Ferroelectr. Freq. Control* **2009**, *56*, 334–344. [PubMed]
5. Hu, Y.; Jiang, X.; Shu, L.; Zhang, Z.; Hu, Q.; Hu, J. DC flashover performance of ice-covered insulators under complex ambient conditions. *IET Gener. Transm. Distrib.* **2016**, *10*, 2504–2511. [CrossRef]
6. Hu, Q.; Wang, S.; Shu, L.; Qiu, G. Comparison of AC icing flashover performances of 220 kV composite insulators with different shed configurations. *IEEE Trans. Dielectr. Electr. Insul.* **2016**, *23*, 995–1004. [CrossRef]
7. Ale-Emran, S.M.; Farzaneh, M. Flashover performance of ice-covered post insulators with booster sheds using experiments and partial arc modeling. *IEEE Trans. Dielectr. Electr. Insul.* **2016**, *23*, 979–986. [CrossRef]
8. Taheri, S.; Farzaneh, M.; Fofana, I. Empirical flashover model of EHV post insulators based on ISP parameter in cold environments. *IEEE Trans. Dielectr. Electr. Insul.* **2016**, *23*, 403–409. [CrossRef]
9. Hu, J.; Yan, B.; Zhou, S.; Zhang, H. Numerical Investigation on Galloping of Iced Quad Bundle Conductors. *IEEE Trans. Power Deliv.* **2012**, *27*, 784–792. [CrossRef]
10. Chadha, J.; Jaster, W. Influence of turbulence on the galloping instability of iced conductors. *IEEE Trans. Power Appl. Syst.* **2006**, *94*, 1489–1499. [CrossRef]
11. Kermani, M.; Farzaneh, M.; Kollar, L.E. The Effects of Wind Induced Conductor Motion on Accreted Atmospheric Ice. *IEEE Trans. Power Deliv.* **2013**, *28*, 540–548. [CrossRef]
12. Yan, B.; Chen, K.; Guo, Y.; Liang, M.; Yuan, Q. Numerical Simulation Study on Jump Height of Iced Transmission Lines After Ice Shedding. *IEEE Trans. Power Deliv.* **2012**, *28*, 216–225. [CrossRef]
13. Kollar, L.E.; Farzaneh, M. Modeling Sudden Ice Shedding from Conductor Bundles. *IEEE Trans. Power Deliv.* **2013**, *28*, 604–611. [CrossRef]

14. Kollar, L.E.; Farzaneh, M. Vibration of Bundled Conductors Following Ice Shedding. *IEEE Trans. Power Deliv.* **2008**, *23*, 1097–1104. [CrossRef]
15. Kannus, K.; Lahti, K. Laboratory investigations of the electrical performance of ice-covered insulators and a metal oxide surge arrester. *IEEE Trans. Dielectr. Electr. Insul.* **2007**, *14*, 1357–1372. [CrossRef]
16. Nygaard, B.E. Evaluation of icing simulations for all the "COST727 icing test stations". In Proceedings of the International Workshop on Atmospheric Icing on Structures (IWAIS 2009), Andermatt, Switzerland, 8–11 September 2009; pp. 1–5.
17. Thompson, G.; Nygaard, B.E.; Makkonen, L. Using the Weather Research and Forecasting (WRF) Model to Predict Ground/Structural Icing. In Proceedings of the International Workshop on Atmospheric Icing on Structures (IWAIS 2009), Andermatt, Switzerland, 8–11 September 2009; pp. 1–8.
18. Lashkarbolooki, S.; Pahwa, A.; Tamimi, A.; Yokley, R. Decreasing the ice storm risk on power conductors by sequential outages. In Proceedings of the 2017 North American Power Symposium (NAPS), Morgantown, WV, USA, 17–19 September 2017; pp. 1–4.
19. Pohlman, J.C.; Landers, P. Present State-of-the-Art of Transmission Line Icing. *IEEE Trans. Power Appl. Syst.* **1982**, *101*, 2443–2450. [CrossRef]
20. Huang, X.; Zhang, F.; Li, H.; Liu, X. An Online Technology for Measuring Icing Shape on Conductor Based on Vision and Force Sensors. *IEEE Trans. Instrum. Meas.* **2017**, *66*, 3180–3189. [CrossRef]
21. Liu, X.; Lang, S.; Zhao, B.; Zhang, F.; Liu, Q.; Tang, C.; Li, D.; Fang, G. High-Resolution Ice-Sounding Radar Measurements of Ice Thickness Over East Antarctic Ice Sheet as a Part of Chinese National Antarctic Research Expedition. *IEEE Trans. Geosci. Remote Sens.* **2018**, *56*, 3657–3666. [CrossRef]
22. Mao, N.; Ma, G.; Li, C.; Du, Y. High sensitive FBG load cell for icing of overhead transmission lines. International Conference on Optical Fiber Sensors. In Proceedings of the 25th International Conference on Optical Fiber Sensors, Jeju, Korea, 24–28 April 2017.
23. Deng, Y.; Xu, T.; Li, Y.; Feng, P.; Jiang, Y. Icing thickness prediction of overhead transmission lines base on combined kernel function SVM. In Proceedings of the 2017 IEEE Conference on Energy Internet and Energy System Integration (EI2), Beijing, China, 26–28 November 2017; pp. 1–4.
24. Ma, Y.; Yu, H.; Liu, J.; Zhai, Y. Measurement of ice thickness based on binocular vision camera. In Proceedings of the 2017 IEEE International Conference on Mechatronics and Automation (ICMA), Takamatsu, Japan, 6–9 August 2017; pp. 162–166.
25. Janíček, F.; Holjenčík, J.; Lend'ák, F.; Gogola, R. The effect of conductor diameter upon the thickness of icing. In Proceedings of the IEEE International Scientific Conference on Electric Power Engineering, Prague, Czech Republic, 16–18 May 2016; pp. 1–4.
26. Chao, Y.; Jiang, X.; Bi, M.; Chen, L.; Zhang, Z.; Shu, L. Diameter correction coefficient of the icing thickness on the conductors. *High Volt. Eng.* **2011**, *37*, 1391–1397.
27. Jiang, X.; Dong, B.; Chao, Y.; Zhang, Z.; Hu, Q.; Hu, J.; Shu, L. Diameter correction coefficient of ice thickness on conductors at natural ice observation stations. *IET Gener. Transm. Distrib.* **2014**, *8*, 11–16.
28. Yang, J.; Zhu, K.; Yin, Q.; Liu, B.; Li, X.; Si, J. Experimental Study on Diameter Correction Coefficient of Standard Ice Thickness on Conductors. *Electr. Power Constr.* **2015**, *36*, 33–37.
29. Lanctot, E.K.; Peterson, E.L.; House, H.E.; Zobel, E.S. Ice Build-up on Conductors of Different Diameters. *Trans. Am. Inst. Electr. Eng. Part III Power Appl. Syst.* **2008**, *78*, 1610–1614. [CrossRef]
30. Xiang, Z.; Jiang, X.; Hu, J.; Chang, H.; Yin, F.; Li, Z. Shape Correction Coefficient of the Icing Thickness on Conductors Under Natural Icing Condition at Xuefeng Mountain Test Station. *High Volt. Eng.* **2014**, *40*, 3606–3611. (In Chinese)
31. Farzaneh, M. *Atmospheric Icing of Power Networks*; Chinese Electric Power Press: Beijing, China, 2010. (In Chinese)